ACS OMEGA

http://pubs.acs.org/journal/acsodf

Article

Performance Enhancement of the Poplar Wood Composites Biomimetic Mineralized by $CaCO_3$

Mengying Zhang, Hang Li, Chi Wang, Zhaohui Wang, Da Liu, Tao Yang, Zebin Deng, and Guangming Yuan*

Cite This: *ACS Omega* 2022, 7, 29465−29474

Read Online

ACCESS | Metrics & More | Article Recommendations

ABSTRACT: Inspired by the natural matrix-mediated biomineralization, wood composites were prepared by vacuum impregnation using the gel effect of sodium alginate (SA) on calcium ions, which improved the mechanical properties, flame retardant, and smoke suppression properties of the wood composites. Fourier transform infrared spectroscopy (FTIR), X-ray diffraction (XRD) and scanning electron microscopy (SEM) confirmed that the SA inducer had promoted the orderly deposition and directional crystallization of calcium carbonate ($CaCO_3$) inside the wood cell walls and intercellular spaces. The density and weight gain rate of the biomimetic mineralized wood showed that $CaCO_3$ effectively adhered to the interior of wood with SA as an inducer. The compressive and flexural strengths were 15.65% and 37.66% higher than those of the control, respectively. Thermogravimetric analysis (TG) proved that SA alleviated the thermal decomposition and complete combustion of the mineralized wood and improved the thermal stability. Microcalorimetry (MCC) and cone calorimetry (CONE) analyses revealed that the maximum heat release rate (HRR), total heat release (THR), and the total smoke production (TSP) rate of the mineralized wood was reduced by 59.51%, 48.52%, and 51.67%, respectively, compared with those of the control. This research demonstrates the in situ synthesis of $CaCO_3$ within the cellular microstructure of the poplar which is using it as a biotemplate. With the enhancement of the flame retardant property and others, the wood composite biomimetic mineralized materials modified by $CaCO_3$ and SA could be utilized more widely in the construction industry or other fields.

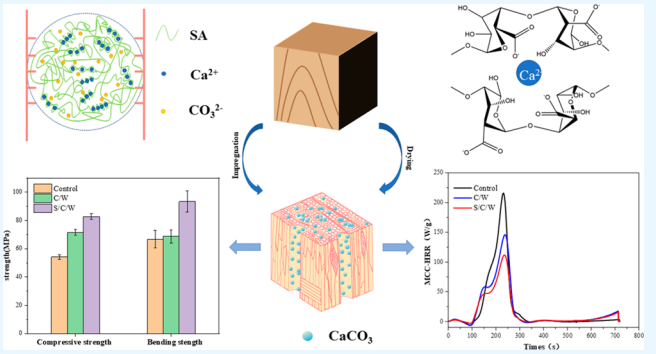

1. INTRODUCTION

Wood has been utilized as a common building material for a very long time, but its flammable property has prompted the search for other fire-resistant alternatives such as concrete, steel, brick and plastic. However, in the event of a fire, steel can cause structural damage or collapse faster than wood.[1] Associated health and environmental concerns arising from the smoke in the fire-field limit the widespread use of wood. Therefore, preparing wood composite with good fire-resistant and smoke suppression effects while enhancing the mechanical properties is necessary. To avoid the quick-burning of wood, a certain amount of flame retardant can be added to inhibit or delay the spread of the fire and the burning process.[2] Flame retardants can be divided into four categories, including phosphorus, halogen, nitrogen, and inorganic flame retardants.[3] However, flame retardants containing halogen or nitrogen and phosphorus elements can release toxic gases during the combustion process, which hurt the human body and the environment.

Calcium carbonate ($CaCO_3$) is a relatively common mineral in nature, and it is widely used as an additive or filler[4] in rubber, plastics, paints and other industrial applications.[5] It is available in three anhydrous forms, namely calcite, vaterite, and aragonite, plus an amorphous $CaCO_3$.[6] Calcite is the most thermodynamically stable structure under environmental conditions. Aragonite and vaterite are generally metastable, which release lower surface energy and transform to calcite slowly.[7] To investigate whether $CaCO_3$ particles are effective flame retardants for wood composites, Yubo et al.[8] prepared composites with $CaCO_3$ and phenolic resin to improve the fire-resistant and mechanical properties of pine flakes. Based on the consideration of environmental protection, Pondelak et al.[9] proposed a new environmental protection method to improve the fire resistance of wood, which is impregnated inside calcium acetate aqueous solution under vacuum pressure and

Received: June 24, 2022
Accepted: July 28, 2022
Published: August 9, 2022

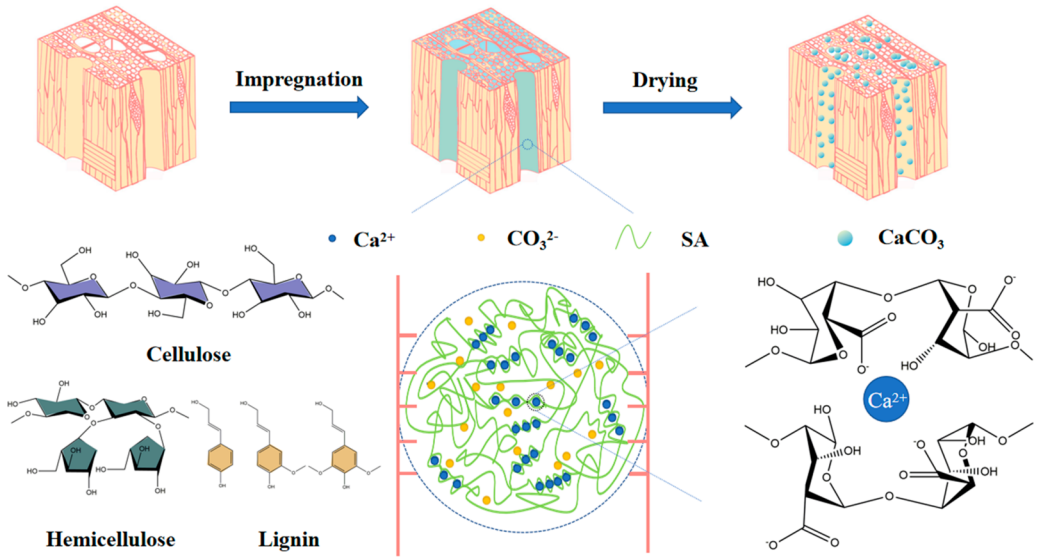

Figure 1. Presentation of the S/C/W.

$CaCO_3$ produced in situ. These studies have proved that $CaCO_3$, as a common inorganic flame retardant, can improve the fire-resistant, smoke suppression and mechanical properties of the wood composites as a more environmentally friendly alternative.[10−12] However, the disadvantage of most technologies reported in the literature is that $CaCO_3$ precipitation usually occurs on the surface of wood, which may hinder the further wood's modifying treatment. Therefore, depositing minerals in the depths of wood remains a major challenge.

Biomineralization is the process by which organisms coordinate the synthesis and organization of the minerals (biominerals).[13] Biomimetic mineralization can control inorganic materials' crystal form and morphology during the nucleation and growth process of inorganic materials by adjusting the ordered structure and spatial configuration of organic matter under the artificial conditions, by which the inorganic materials can be used to in situ modify composites. In the biomimetic synthesis process, various natural or synthetic polymers are used as the templates to control the nucleation and assembly of $CaCO_3$ crystals.[14−16] Inspired by the natural matrix-mediated biomineralization, Merk et al.[17] obtained organic−inorganic hybrid wood composites which significantly reduced the heat release and smoke production by directional deposition of $CaCO_3$, taking advantage of the wood nanoporous cell wall structure. Guo et al.[18] promoted the growth of struvite minerals inside the wood by ammonia fumigation, inhibited heat release rate, smoke production, and improved flame retardancy. These demonstrated the potential application of biomineralization for wood modification and functionalization through scalable nanotechnology.

Sodium alginate (SA) is widely used for biomimetic mineralization, but there are few reports on its application in wood. SA is an anionic polysaccharide that is biodegradable, has good biocompatibility and is bioactive. It is not only cheap but also possesses a gelling ability and can be combined with divalent or trivalent cations such as Ca^{2+} and Fe^{3+} etc. to form an egg-box structure.[19] Araújo et al.[20] employed the gelling properties of alginate to synthesize micro/nano CaO. The process is environment-friendly, during which CO_2 and H_2O as the main final byproducts. Jun et al.[21] investigated the effect of the biological polysaccharide sodium alginate on the morphology and polymorphism of $CaCO_3$ and realized the biomimetic regulation of microbially induced calcium carbonate precipitation (MICP). These results were consistent with the principle of biomineralization and provided a specific theoretical basis for the preparation of SA to induce the in situ generations of $CaCO_3$ in wood.

In this work, we demonstrate the in situ synthesis of $CaCO_3$ within the wood cellular microstructure using poplar as a biological template. The molecular chain of SA contains a large number of hydroxyl groups, which are not only allowed for SA's formation in the wood cell wall or intercellular space but also can be used as a carbon source in an intumescent flame retardant system to improve the carbon form in the system. Based on the biomineralization principle, SA is used to induce the synthesis of $CaCO_3$ in the wood and improve the mechanical, fire-resistant, and smoke suppression properties of the wood composites.

2. MATERIALS AND METHODS

2.1. Materials. A fast-growing poplar tree was cut into several pieces (in the longitudinal, radial, and chordal directions) to different sizes for different test operations. These are 30 mm × 30 mm × 5 mm (powder sample preparation), 20 mm × 20 mm × 20 mm (wood density and weight gain tests), 300 mm × 20 mm × 20 mm (bending strength test), 30 mm × 20 mm × 20 mm (compressive strength test), 100 mm × 100 mm × 6 mm (cone calorimetry test). SA was provided by Tianjin Guangfu Fine Chemical Co.; sodium hydroxide (NaOH) was provided by Beijing Cool Chemical Technology Co.; calcium chloride dihydrate ($CaCl_2 \cdot 2H_2O$), and ammonia carbonate ($(NH_4)_2CO_3$) were provided by Sinopharm Chemical Reagent Co.

2.2. Wood Pretreatment. The wood samples were washed using deionized water and then dried in an oven. The dried poplar wood was placed in a 2% (mass fraction) NaOH solution for 10 h at room temperature. The activity of the poplar wood is improved because of the breaking of the hydrogen bonds of the cellulose in the wood by the sodium-hydroxide solution and releasing the free hydroxyl groups.

2.3. Preparation of the S/C/W Sample. First, 1% SA was dissolved in an aqueous solution and heated at 80 °C for 30

https://doi.org/10.1021/acsomega.2c03960
ACS Omega 2022, 7, 29465−29474

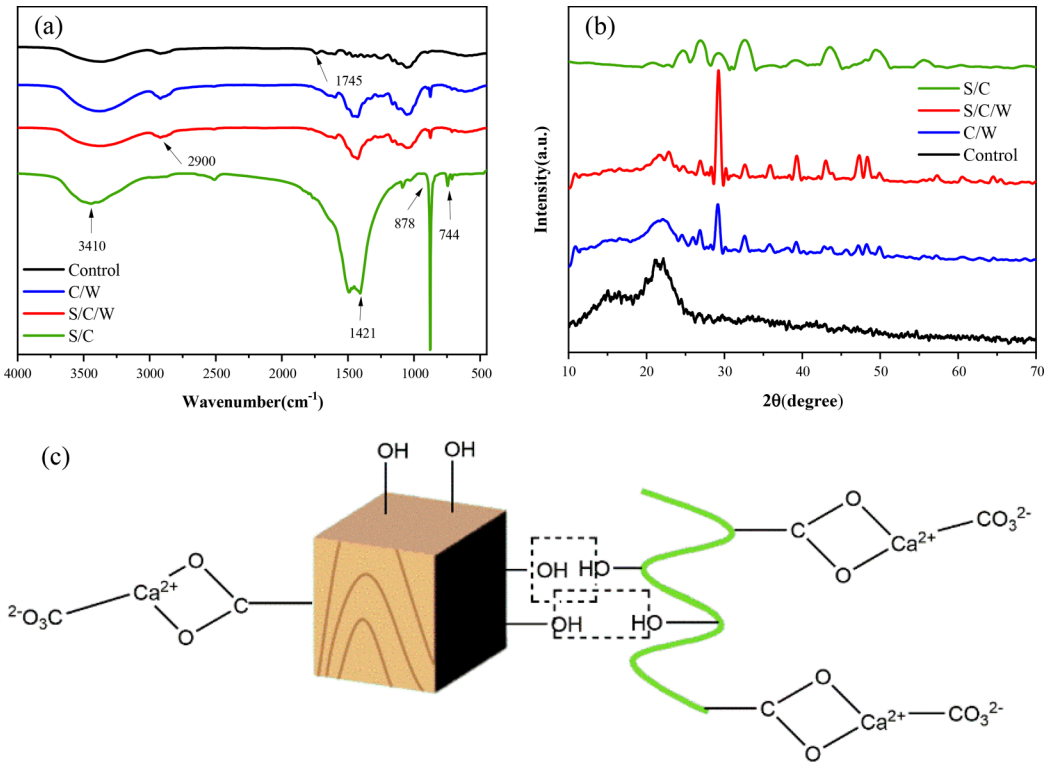

Figure 2. FTIR spectra (a), XRD pattern (b), mechanistic diagram of S/C/W (c).

min to obtain the SA solution. The pretreated wood was then placed in SA solution, the pressure was set at 0.5 MPa, and the pretreated wood was impregnated in a vacuum for 8 h. Next, the wood was impregnated with a configured calcium chloride solution at a concentration of 1 mol/L at a pressure of 0.5 MPa for 8 h. Third, the wood was impregnated using an ammonium carbonate solution at 1 mol/L concentration and 0.5 MPa pressure for 8 h. Ammonia production leads to an increase in the pH in the environment, which favored the precipitation of $CaCO_3$ in a calcium-rich environment. Finally, the wood was cleaned from the surface solution and dried in an oven. The obtained dried wood was S/C/W. For comparison, C/W without SA was studied according to the above steps. The untreated wood was denoted as Control. The preparation mechanism is shown in Figure 1.

2.4. Performance Characterization. *2.4.1. Fourier-Transform Infrared Spectroscopy (FTIR).* The chemical structure of the wood samples was analyzed using infrared spectroscopy (IRAffinity-1, Shimadzu Co. Ltd., Japan). Powder samples (5−10 mg) with a particle size of 200 mesh were completely dried at 105 °C for 12 h before testing. The FTIR spectra ranged from 400 to 4000 cm^{-1}.

2.4.2. X-ray Diffraction (XRD). The crystal structure of the treated wood samples was examined using an X-ray diffractometer (XPert, Dutch Co. Ltd. Netherlands). Scans were taken in the 2θ range from 10° to 70° diffraction angle at a speed of 4°/min.

2.4.3. Scanning-Electron Microscopy (SEM). A field emission scanning electron microscope with an energy dispersive X-ray analysis unit (MIRA3 LMH, FEI Co. Ltd., U.S.A.) was used in this study to observe the morphology and microstructure of the wood samples. All tested were coated with platinum for 20 min, and the measurement voltage was 15 kV.

2.4.4. Physical and Mechanical Properties. The physical and mechanical properties of the wood samples were tested in accordance with the Chinese National Standard Test Method for Physical and Mechanical Properties of Wood (GB/T 1929−2009). Cubic samples of 20 mm × 20 mm × 20 mm ($R \times T \times L$) to test the weight gain (WPG) and density. Before impregnation, the specimens were baked to absolute dryness and weighed and then baked again to absolute dryness after the impregnation was completed. The WPG of the samples was calculated as follows

$$\mathrm{WPG}(\%) = (M_2 - M_1)/M_1 \times 100$$

where M_1 is the absolute dry quality of the wood in the blank control group, g; M_2 is the absolute dry mass of the wood after impregnation treatment, g.

The specimen density was calculated using the following equation

$$\rho = M/V$$

where ρ is the density of the specimen when it is absolutely dry, g·cm^{-3}; M is the mass of the sample when it is absolutely dry, g.

The wood mechanical properties of the wood were evaluated by determining the bending strength (MOR) and the compressive strength (CS) of the parallel grains. Bending strength tests were performed according to the Chinese National Standard GB/T 1936−2009, and CS tests were performed according to the Chinese National Standard GB/T 1935−2009. Specimen sizes of 20 mm × 20 mm × 300 mm ($R \times T \times L$) were used for the MOR test, and sizes of 20 mm × 20 mm × 30 mm ($R \times T \times L$) were used for the CS test. The MOR was investigated under static three-point bending conditions using an AG-type universal testing machine (2000A, Shimadzu Corporation, Japan).

https://doi.org/10.1021/acsomega.2c03960
ACS Omega 2022, 7, 29465−29474

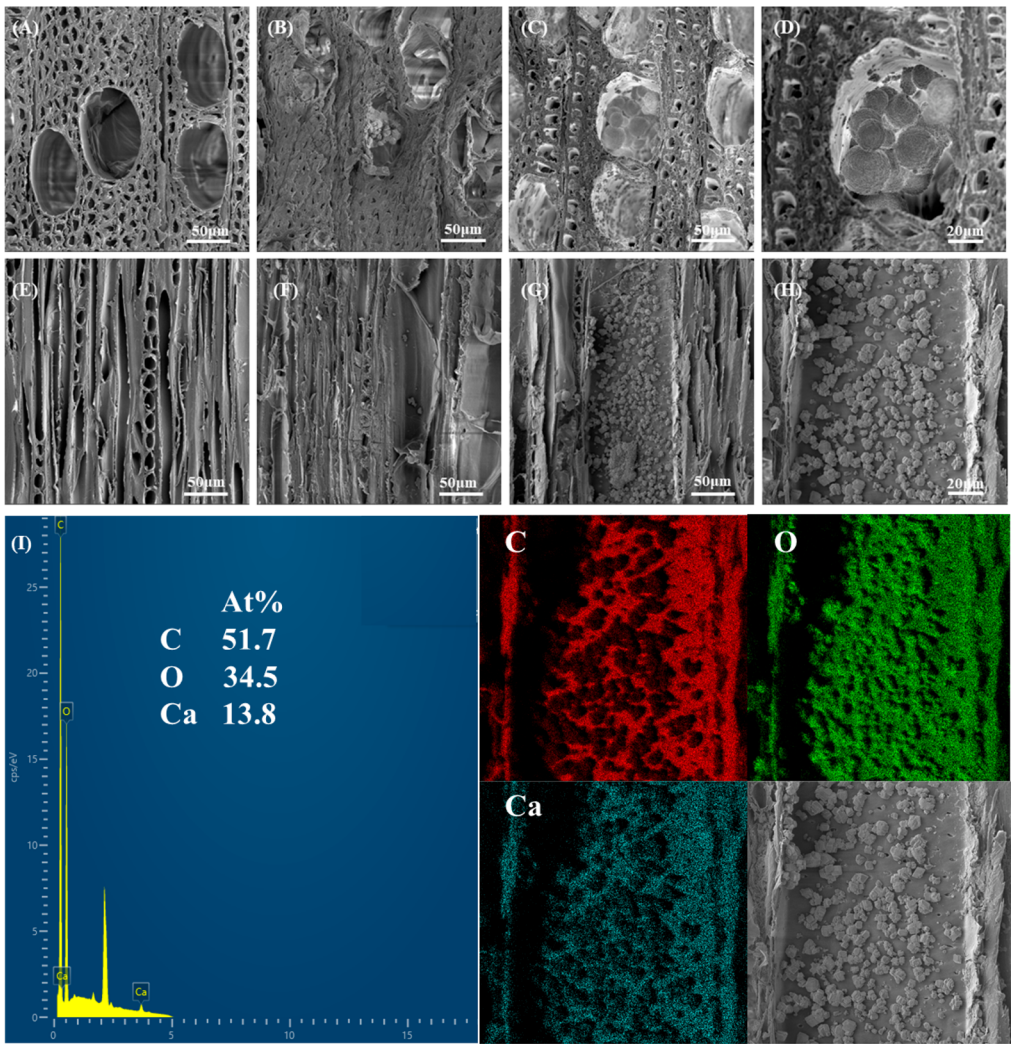

Figure 3. SEM images and EDS spectrum of control and mineralized wood (A,E, the control; B,F, C/W; C,D,G,H, S/C/W; I, EDS spectrum of S/C/W).

2.4.5. Thermogravimetric Analysis (TGA). A thermogravimetric analyzer (TG-DTA7300, Seiko Co. Ltd., Japan) was used to determine the thermal stability of the wood samples. All sample powders were tested after being completely dried at 105 °C for 12 h. Wood sample powders with a particle size of 200 mesh or less were heated to 800 °C under nitrogen at 80 mL/min and in an air atmosphere at a rate of 10 °C/min to analyze the thermal stability of the mineralized wood.

2.4.6. Cone Calorimeter (CONE) and Miniature Combustion Calorimeter (MCC). CONE (FTT, Stanton Redcroft Ltd., U.K.) and MCC (MCC-2, Gomak Co. Ltd., U.S.A.) were used to analyze the flame-retardant properties of the mineralized wood. All wood samples (100 mm × 100 mm × 5 mm) were tested after complete drying at 105 °C for 24 h. A wood powder (10−15 mg) test was performed under a nitrogen atmosphere from 30 to 750 °C at 1 °C·min^{-1}. For the MCC measurements, the samples were tested at a heating rate of 1 °C/s.

3. RESULTS AND DISCUSSION

3.1. Chemical Structure Analysis. FTIR spectroscopy was performed to analyze the difference in the chemical functional groups between the control, C/W and S/C/W. The results are shown in Figure 2a. The FTIR spectra of the control, C/W and S/C/W were approximately similar, which indicated that the modification treatment did not destroy the wood structure itself. As shown in Figure 2a, the absorption peak of the hydroxyl group was approximately 3410 cm^{-1},[22] and −OH could be attributed to the existence of hydroxyl groups in the cellulose, hemicellulose, and lignin in the wood.[23] The complete disappearance of the peak at 1745 cm^{-1} indicated complete hemicellulose degradation. Previous studies demonstrated that nanopores were observed in the S_2 layer of the cell wall after partial removal of lignin and hemicellulose, which indicated increased porosity of the wood and allowed easier access of the precursor solution to the wood cell wall.[24] Compared with the control, the −OH absorption peak bands of C/W and S/C/W became deep, indicating that the hydroxyl groups on the wood surface were activated by the NaOH treatment. The −OH absorption peak intensity of S/C/W was lower than that of C/W because some hydroxyl groups of SA reacted with the hydroxyl groups in the wood. The absorbance band at 1421 cm^{-1} were $v_{3-3}CO_3^{2-}$ and $v_{3-4}CO_3^{2-}$,[25] indicating that $CaCO_3$ was in situ generated inside the wood. The new absorption peaks around 878 and 744 cm^{-1} were the absorption peaks of calcite calcium carbonate,[26] which further indicated that the polycrystalline form of $CaCO_3$ in the composite material was calcite. Compared with that of

https://doi.org/10.1021/acsomega.2c03960
ACS Omega 2022, 7, 29465−29474

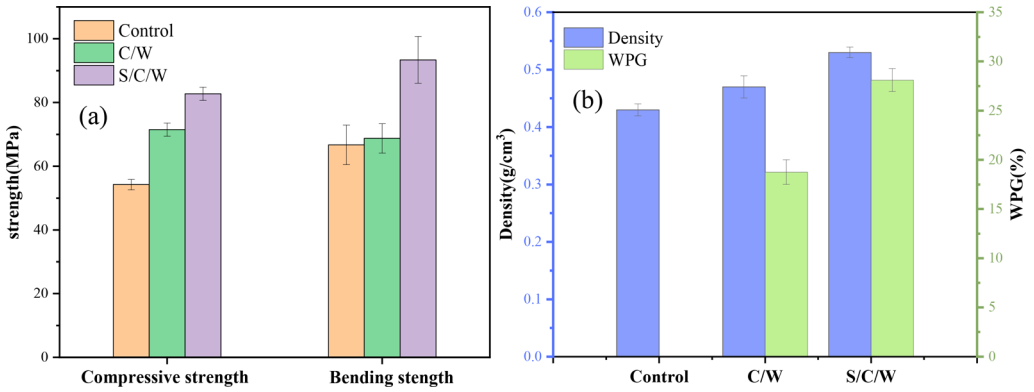

Figure 4. Compressive and bending strength of the control, C/W, and S/C/W (a); density and WPG of control, C/W, and S/C/W (b)

the C/W wood, the CO_3^{2-} absorption peak band of the S/C/W wood was smaller at approximately 878 cm^{-1}, which could be due to the formation of a complex reaction between the carboxylic acid ions of SA and the calcium ions,[27] which affected the diffusion process of CO_3^{2-} and calcium ions in the wood, and induced nucleation and growth of the $CaCO_3$ crystal to a certain extent. The organic−inorganic hybrid structure is shown in Figure 2c.

The crystal structure and phase analyses of the control and modified wood were carried out using an X-ray diffractometer. Figure 2b shows that obvious cellulose characteristic diffraction peaks appeared at 2θ of 17° and 22.0°. After the wood was impregnated, the cellulose crystallinity decreased with higher precursor concentration, and the characteristic peaks of the cellulose gradually weakened. It is evident that in addition to the typical crystal face of the cellulose, the mineralized wood also contained various crystal types such as calcite, spheraragonite, and aragonite, and the crystal type of $CaCO_3$ was mainly calcite with the highest thermodynamic stability. Both C/W and S/C/W samples showed obvious calcite-type (29.19°, 39.29°, 47.33°, and 48.42° at 2θ) and characteristic diffraction peaks of aragonite-type $CaCO_3$ (26.97° and 32.76°). It can be clearly seen that the S/C/W contained more calcite calcium carbonate. The crystallinity of the crystal can be understood by observing the sharpness of the diffraction peak. The sharper the diffraction peak was, the higher the crystallinity of the particles.[28] Comparing the C/W and S/C/W samples reveals that the S/C/W exhibited the sharpest diffraction peak and highest particle crystallinity, which indicated that SA successfully induced $CaCO_3$ to enter the wood cell wall and generated $CaCO_3$ carbonate with the highest stability.

3.2. Microstructure Analysis. The distribution of minerals in the control, C/W and S/C/W were investigated using SEM and EDS. Figure 3A depicts a cross-section of the control with high porosity. In contrast to the rare $CaCO_3$ content on C/W (Figure 3B), some of the tube holes in the S/C/W (Figure 3C,D) were filled with $CaCO_3$, which made the original honeycomb structure of the wood denser. The process not only improved the wood density but also reduced the oxygen content of the wood, which was crucial for improving the flame retardant performance.[29] Figure 3E shows a cut surface of the control. It was almost no $CaCO_3$ deposition on the string section of C/W (Figure 3F), while $CaCO_3$ can be clearly seen deposited on the pipes and pits in the wood rays in the S/C/W (Figure 3G,H), indicating that during the impregnation process, the SA solution can be circulated in the wood pipes and wood rays to achieve a good deposition modification effect. These results demonstrated that the reactive groups in the SA provided nucleation sites for $CaCO_3$ and promoted the rapid deposition directional crystallization of $CaCO_3$ in the wood cell walls and voids. As reported by Merk et al.,[17] the deposition pattern of $CaCO_3$ minerals appeared to be consistent with the microporous structure in the wood that facilitated fluid transport.

Energy dispersive spectroscopy (EDS) is an elemental analysis used in conjunction with SEM to analyze the elemental composition of additives to visualize the elemental composition of the S/C/W. The EDS map evidently indicated that the distribution of elemental carbon and oxygen followed the profile of the cell wall, which may have come from the cell wall polymers or composites. In addition to C and O, a Ca signal was also detectable at recognizable levels, and it appeared to be evenly distributed throughout the cell wall at 13.8%. Elemental Ca originated from the $CaCl_2$ solution, which is likely to form an ionically cross-linked gel with the GG-dimer structure of SA,[30] thereby inducing in situ mineralization of $CaCO_3$ in the wood cell wall and lumens and enhancing the wood mechanical performance and flame retardant properties.

3.3. Analysis of Physical and Mechanical Properties. The results of the mechanical properties of each sample are shown in Figure 4. The compressive strength and bending strength of the control were 54.24 and 67.85 MPa, respectively. Compared with the control, the density of C/W increased from 0.43 to 0.47 g/cm^3, with a weight gain of 18.75% and a significant increase in compressive strength to 31.82%. Meanwhile, no significant change occurred in bending strength. It shows that after the hydrothermal impregnation, $CaCO_3$ precipitates were formed in the wood by ionic reactions, which filled the cellular cavities and pores of the wood and increased its compressive strength. The mechanical properties of wood have been well-known to be closely related to its density.[31] S/C/W has 23.26% higher density, 28.10% higher weight gain, 37.66% higher flexural strength, and 52.52% higher compressive strength compared to the control. Therefore, we could assume that SA acted as an inducer to form hydrogen or chemical bonds with the functional groups of the wood components and the hydroxyl groups on the surface of the $CaCO_3$. On the other hand, the carboxylate ions of SA created complexation reactions with Ca^{2+}, which induced $CaCO_3$ deposits in the cell walls and cell cavities of the wood, allowed the mineral to resist external deformation together with the cell walls and improved the wood bending strength.

https://doi.org/10.1021/acsomega.2c03960
ACS Omega 2022, 7, 29465−29474

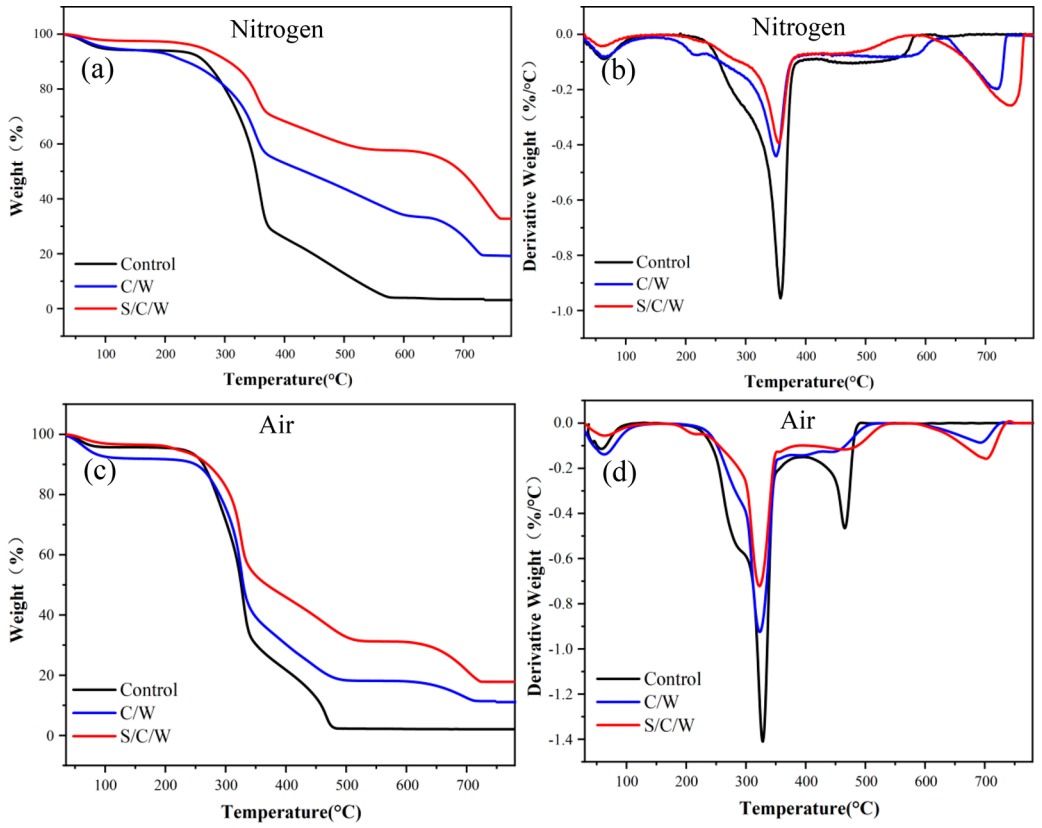

Figure 5. TGA and DTG curves of the control, C/W, and S/C/W (a,b, under nitrogen; c,d, under air).

Table 1. TGA Data Table of the Control, C/W, and S/C/W[a]

	nitrogen			air		
sample	$T_{10\%}$ (°C)	T_{max} (°C)	residue at 800 °C(%)	$T_{10\%}$ (°C)	T_{max} (°C)	residue at 800 °C(%)
Control	266.62	355.67	3.49	262.95	328.73	2.05
C/W	235.31	352.05	19.17	250.16	324.72	11.38
S/C/W	306.47	353.79	32.74	270	324.55	17.79

[a] $T_{10\%}$ refers to the temperature at which pyrolysis weight loss is 10%

3.4. Thermal Stability Analysis. TGA was used to analyze the thermal stability of the control and mineralized wood. The TGA and DTA curves of the control and mineralized wood samples are depicted in Figure 5, and the relevant data are presented in Table 1. For the control, there is a derivative weight peak at 50° between room temperature and 120 °C due to the evaporation of water absorbed by the wood cell walls. After this, the wood fraction underwent pyrolysis, in which the hemicellulose first decomposed at ~240 °C due to its thermal instability, and a slight shoulder peak could be seen in the DTG curve. The most prominent peak in the DTG curve occurred at approximately ~360 °C, which represented the stage in which cellulose degradation of the control was predominant. However, the degradation range of lignin was much wider, from approximately 260 to 500 °C. The complete pyrolysis of the wood fraction at 800 °C resulted in a weight loss of 96% and a final residue of 3.49%.

From the DTG curves, it can be found that the hemicellulose and cellulose degradation peaks in the DTA curves of the control were suppressed to different degrees in both C/W and S/C/W. In addition, the temperature required for C/W weight loss to reach 10% was lower than the control. This result could probably be attributed to the fact that during the treatment of the wood chips with aqueous NaOH solutions, the alkali solution penetrated into the voids of the chips and internally diffused, which reacted with the functional groups such as glucuronic acid, esters, and acetyl groups of the wood components consumed a certain amount of hemicellulose and removed some impurities from the surface of the wood fibers.[32] Therefore, more voids were exposed to heat and reached the surface of the wood components, leading to rapid decomposition of the wood. The final residual carbon ratio of C/W was calculated to be 19%, which could be due to $CaCO_3$ that, as a weak base, catalyzed the decomposition or depolymerization of pyrolytic cellulose, increased the formation of coke and improved thermal stability.

For the S/C/W samples, it is worth noting that the addition of small amounts of SA exerted a significant effect on the thermal behavior and residual carbon rate of the mineralized wood. Figure 5a shows that the thermal burning of the control in the second stage was clearly suppressed from approximately 260 to 360 °C compared with that in the C/W sample. These results demonstrated how SA reacted with the cellulose in the wood, and caused biomolecular chains to grow, which acted as an insulating fire barrier, prevented oxygen from contacting the wood, reduced the rate of wood thermal decomposition,

https://doi.org/10.1021/acsomega.2c03960
ACS Omega 2022, 7, 29465−29474

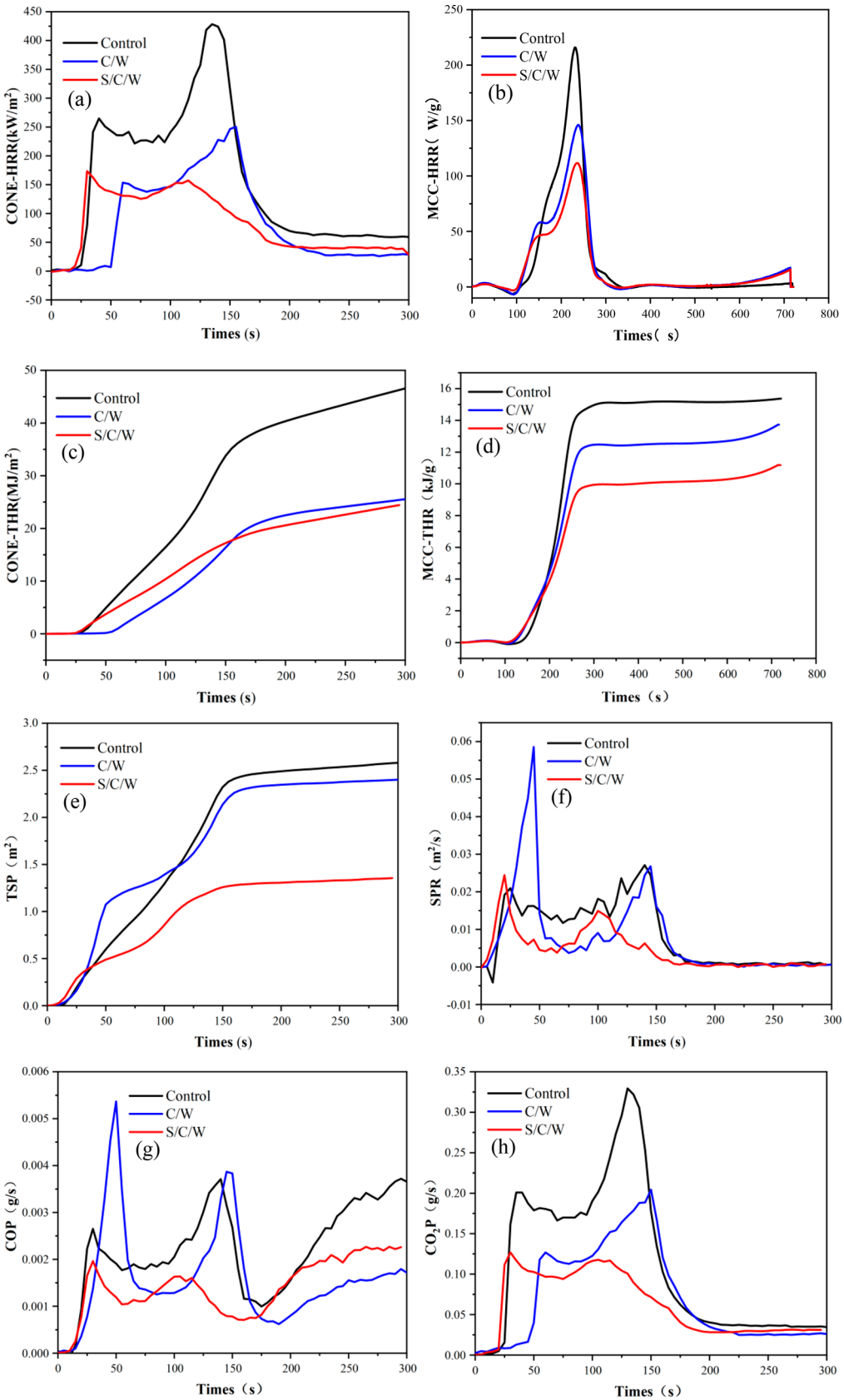

Figure 6. CONE and MCC curves of the control, C/W and S/C/W (a, CONE-HRR; b, MCC-HRR; c, CONE-THR; d, MCC-HRR; e, TSP; f, SPR; g, COP; h, CO_2P).

inhibited the release of gases and volatile fractions during the second stage of pyrolysis and increasing the residual carbon rate of S/C/W. From 380 to 580 °C, $CaCO_3$ formed an inorganic carbon layer structure on the wood surface, which

https://doi.org/10.1021/acsomega.2c03960
ACS Omega 2022, 7, 29465−29474

impeded the transfer of mass during the wood pyrolysis and further reduced the rate of wood pyrolysis, with a final mass residual carbon rate of 32%. The comparative analysis of the residual carbon rate in the Table 1 shows that since the thermal decomposition temperature of $CaCO_3$ at high temperature is about 800 °C, the content of $CaCO_3$ in the test under N_2 atmosphere remains unchanged, and the remaining $CaCO_3$ content in S/C/W is calculated to be 29.25%, while the C/W is 15.68%, so the content of $CaCO_3$ induced by SA inside the wood is higher than that of simple impregnation of $CaCO_3$ was elevated by 86.54%, which greatly enhanced the mineralization efficiency.

The pyrolysis of wood in an air atmosphere was divided into three stages. The first two stages were similar to pyrolysis under a nitrogen atmosphere. However, in the third stage, the wood's hemicellulose and lignin molecular products were further oxidized and decomposed because of the presence of oxygen, which eventually produced a residue of 2.05%. Meanwhile, the residual carbon rates of C/W and S/C/W were 11.38% and 17.79%, respectively. Figure 5c shows that the pyrolytic behavior of the mineralized wood was inhibited in varying degrees at different stages compared with that in the control. The S/C/W samples were more strongly inhibited than C/W, indicating that the carbon layer structure formed by the combination of SA and $CaCO_3$ was denser than that of the precursor solution impregnated with $CaCO_3$ alone, which remarkably prevented further oxygen penetration into the char structure, reducing the heat transfer and the release of combustible gases and improved the wood thermal stability.

3.5. Flame Retardant Performance. The combustion behavior of the control and mineralized wood in real fire scenarios was characterized using a combination of CONE and MCC. Figure 6 shows the control exhibited two maximum heat release rate (HRR) peaks. The first was 264.74 kW/m^2 because the sufficient heat generated volatile gases from the decomposition of hemicellulose, cellulose, and lignin within the wood. As the combustion continued, an adiabatic char layer formed on the surface of the wood, which slowed down the rate of heat release because of the difficulty in the heat transfer through the adiabatic char layer. Following the cracking of the charcoal layer, the flammable gas was rereleased, which led to a second peak that reached a maximum value of 428.35 kW/m^2, as listed in Table 2. After the volatiles had burned out, the HRR curve reached a plateau. The peak HRR (pHRR) and the total heat release (THR) reflected the rate and some of the heat released from the material from ignition to extinction, respectively.[33] The control group reached the highest pHRR and THR of 428.35 kW/m^2 and 47.38 MJ/m^2, respectively.

Table 2. Data Table of CONE[a]

sample	TTI (s)	pHRR (kW/m^2)	Mean-HRR (kW/m^2)	THR (MJ/m^2)	TSP (m^2)
Control	25	428.35	163.36	47.38	2.40
C/W	48	250.57	96.27	26.03	1.52
S/C/W	21	173.42	89.89	24.39	1.16

[a]TTI (time to ignition), pHRR (peak heat release rate), Mean-HRR (mean heat release rate), THR (total heat release), TSP (total smoke production).

As expected, the pHRR and THR values of all the mineralized wood were lower than those of the control. The pHRR of C/W was reduced by 41.51% compared with that of the control. In addition to the ignition time, the slope and value of the THR curve could also be used as an indicator of slow ignition.[33] The slope of the THR curve of C/W was clearly reduced, in which THR decreased from 47.38 MJ/m^2 to 26.03 MJ/m^2, suggesting that $CaCO_3$ is a noncombustible inorganic material that could effectively reduce the heat release of combustible gases by forming a dense protective layer on the surface of the wood as it adheres to the wood surface.[8]

The first phase of S/C/W reached a maximum HRR value of 173.42 kW/m^2, which was 34.48% lower than the first peak value of the control because of the interaction between SA and the cellulose and hemicellulose in the wood, and thus reduced the oxidative decomposition of cellulose and hemicellulose. Over time, a second exothermic peak of 157.26 kW/m^2 occurred, which was 72.55% lower than that of the control, where SA and $CaCO_3$ in the mineralized wood formed a dense charcoal layer structure that gradually transferred to the surface of the wood, and prevented further heat transfer. These results were consistent with the previous TG data. The pHRR value was 59.51% lower than that of the control and 30.78% lower than that of C/W, which indicated that the wood was effectively treated with SA to reduce its porosity and filled with more $CaCO_3$. This process greatly reduced the rate of thermal degradation to generate flammable, volatile products. The reduction in the heat was beneficial for the feedback of the wood, and the flame retardant effect was noticeable. The graph shows that the THR value of S/C/W was 48.52% lower than that of the control, indicating that SA significantly affected the inhibition of heat release from wood. In terms of the THR, S/C/W was smaller than C/W, which indicated that S/C/W achieved a much milder burning performance than C/W.

As wood is often used in interior construction, furniture, or decorative wood materials, smoke suppression is also an important property. According to Table 2, the smoke production ratio (SPR) and total smoke production (TSP) were lower than those of the control. In Figure 6, TSP and SPR of C/W reached their peak values before 50 s, which might have been caused by the ammonium carbonate solution that remained in the wood during the impregnation process. After drying, the residues decomposed due to thermal instability and generated ammonia gas, carbon dioxide, and other gases that caused a rapid increase in the smoke release rate. Combined with the data in Table 2, the TSP of C/W and S/C/W samples decreased by 36.67% and 51.67%, respectively, compared to the control, and S/C/W showed better smoke suppression performance. In addition, from the perspective of environmental protection, CO and CO_2 emissions could bring a negative effect on the human body and the environment. The chart shows that the S/C/W inhibited CO and CO_2 emissions in varying degrees.

4. CONCLUSION

In conclusion, we have proposed a method for improving the in situ generations of $CaCO_3$ in wood, namely, impregnating SA under vacuum conditions to induce the in situ generations of $CaCO_3$ in the wood to improve fire-resistant and smoke suppression properties. The SEM, FTIR and XRD analyses confirmed that SA successfully entered the wood cell wall micropores and induced the in situ generations of $CaCO_3$. The density increase rate, WPG, compressive strength and bending strength of the $CaCO_3$ mineralized wood induced by SA were improved to varying degrees, regardless of whether it was

https://doi.org/10.1021/acsomega.2c03960
ACS Omega 2022, 7, 29465−29474

compared with the control or the precursor solution simply impregnated with $CaCO_3$. TGA proved that SA and $CaCO_3$ could form a denser carbon layer structure and improve thermal stability. In the MCC and CONE data, the maximum HRR gradually decreased. Therefore, the hybrid material formed by the gelling ability possessed the ability to reduce the total heat of combustion, which improved the mechanical properties and thermal stability of wood.

Compared with the traditional impregnation of $CaCO_3$ precursor solution, in our proposed method, $CaCO_3$ particles induced by SA could not possibly accumulate on the wood surface and block the pores, thus affecting the subsequent impregnation process thereby improving the efficiency of $CaCO_3$ formation in the wood structure. The other was a simple impregnation process in which a renewable green material was converted in situ inside the wood during preparation into a final product without any byproducts. The promised method embedded $CaCO_3$ in the wood using biomimetic mineralization, which provided a path for future industrial applications of wood composites.

AUTHOR INFORMATION

Corresponding Author

Guangming Yuan − *School of Materials Science and Engineering, Central South University of Forestry and Technology, Changsha 410011 Hunan, China; Collaborative Innovation Center for Effective Utilizing of Wood and Bamboo Resource of China, Changsha 410004 Hunan, China;* orcid.org/0000-0002-3609-5369; Email: ygm@csuft.edu.cn

Authors

Mengying Zhang − *School of Materials Science and Engineering, Central South University of Forestry and Technology, Changsha 410011 Hunan, China*

Hang Li − *School of Materials Science and Engineering, Central South University of Forestry and Technology, Changsha 410011 Hunan, China*

Chi Wang − *School of Materials Science and Engineering, Central South University of Forestry and Technology, Changsha 410011 Hunan, China*

Zhaohui Wang − *School of Materials Science and Engineering, Central South University of Forestry and Technology, Changsha 410011 Hunan, China*

Da Liu − *School of Materials Science and Engineering, Central South University of Forestry and Technology, Changsha 410011 Hunan, China*

Tao Yang − *School of Materials Science and Engineering, Central South University of Forestry and Technology, Changsha 410011 Hunan, China*

Zebin Deng − *School of Materials Science and Engineering, Central South University of Forestry and Technology, Changsha 410011 Hunan, China*

Complete contact information is available at: https://pubs.acs.org/10.1021/acsomega.2c03960

Funding

National Key Research and Development Program of China, Grant/Award Number: 2019YFE0114600; National Natural Science Foundation of China, Grant/Award Numbers: 32171708, 31770606.

Notes

The authors declare no competing financial interest.

REFERENCES

(1) Wimmers, G. Wood: a construction material for tall buildings. *Nat. Rev. Mater.* **2017**, *2*, 1−2.

(2) Toldy, A.; Niedermann, P.; Szebenyi, G.; Szolnoki, B. Mechanical properties of reactively flame retarded cyanate ester/epoxy resin blends and their carbon fiber reinforced composites. *Express Polym. Lett.* **2016**, *10*, 1016−1025.

(3) Malucelli, G. Textile finishing with biomacromolecules: A low environmental impact approach in flame retardancy. In *The Impact and Prospects of Green Chemistry for Textile Technology*; Woodhead Publishing; 2019; pp 251−279.

(4) Liang, J.; Wang, F. Flexural and impact properties of POM/EVA/HDPE blends and POM/EVA/HDPE/nano-$CaCO_3$ composites. *Polym. Bull.* **2015**, *72*, 915−929.

(5) Srivabut, C.; Ratanawilai, T.; Hiziroglu, S. Effect of nanoclay, talcum, and calcium carbonate as filler on properties of composites manufactured from recycled polypropylene and rubberwood fiber. *Constr. Build. Mater.* **2018**, *162*, 450−458.

(6) Tobler, D. J.; Rodriguez-Blanco, J. D.; Dideriksen, K.; Bovet, N.; Sand, K. K.; Stipp, S. L. S. Citrate Effects on Amorphous Calcium Carbonate (ACC) Structure, Stability, and Crystallization. *Adv. Funct. Mater.* **2015**, *25*, 3081−3090.

(7) Abebe, M.; Hedin, N.; Bacsik, Z. Cryst. Spherical and Porous Particles of Calcium Carbonate Synthesized with Food Friendly Polymer Additives. *Growth Des.* **2015**, *15*, 3609−3616.

(8) Tao, Y.; Li, P.; Cai, L. P.; Shi, S. Q. Flammability and mechanical properties of composites fabricated with $CaCO_3$-filled pine flakes and Phenol Formaldehyde resin. *Compos. B. Eng.* **2019**, *167*, 1−6.

(9) Pondelak, A.; Škapin, A. S.; Knez, N.; Knez, F.; Pazla, T. Improving the flame retardancy of wood using an eco-friendly mineralisation process. *Green Chem.* **2021**, *23*, 1130−1135.

(10) Qu, H.; Wu, W.; Jiao, Y.; Xu, J. Thermal behavior and flame retardancy of flexible poly (vinyl chloride) treated with $Al(OH)_3$ and ZnO. *Polym. Int.* **2005**, *54*, 1469−1473.

(11) Jiang, J.; Li, J.; Gao, Q. Effect of flame retardant treatment on dimensional stability and thermal degradation of wood. *Constr. Build. Mater.* **2015**, *75*, 74−81.

(12) Jimoh, O. A.; Ariffin, K. S.; Bin Hussin, H.; Temitope, A. E. Synthesis of precipitated calcium carbonate: a review. *Carbonate. Evaporite.* **2018**, *33*, 331−346.

(13) Prasad Shastri, V. Biomineralization: A confluence of materials science, biophysics, proteomics, and evolutionary biology. *MRS Bull.* **2015**, *40*, 473−477.

(14) Falini, G.; Albeck, S.; Weiner, S.; Addadi, L. Control of Aragonite or Calcite Polymorphism by Mollusk Shell Macromolecules. *Science* **1996**, *271*, 67−69.

(15) Rautaray, D.; Kumar, P. S.; Wadgaonkar, P. P.; Sastry, M. Highly Versatile Free-Standing Nano-Gold Membranes as Scaffolds for the Growth of Calcium Carbonate Crystals. *Chem. Mater.* **2004**, *16*, 988−993.

(16) Aizenberg, J.; Muller, D. A.; Grazul, J. L.; Hamann, D. R. Direct Fabrication of Large Micropatterned Single Crystals. *Science* **2003**, *299*, 1205−1208.

(17) Merk, V.; Chanana, M.; Gaan, S.; Burger, I. Mineralization of wood by calcium carbonate insertion for improved flame retardancy. *Holzforschung* **2016**, *70*, 867−876.

(18) Guo, H.; Lukovic, M.; Mendoza, M.; Schleputz, C. M.; Griffa, M.; Xu, B.; Gaan, S.; Herrmann, H.; Burgert, I. Bioinspired Struvite Mineralization for Fire-Resistant Wood. *ACS Appl. Mater. Interfaces* **2019**, *11*, 5427−5434.

(19) Mookhoek, S. D.; Fischer, H. R.; Van Der Zwaag, S. Alginate fibres containing discrete liquid filled vacuoles for controlled delivery of healing agents in fibre reinforced composites. *Compos. Part A Appl. Sci. Manuf.* **2012**, *43*, 2176−2182.

(20) dos Santos Araujo, P.; Belini, G. B.; Mambrini, G. P.; Yamaji, F. M.; Waldman, W. R. Thermal degradation of calcium and sodium alginate: A greener synthesis towards calcium oxide micro/nanoparticles. *Int. J. Biol. Macromol.* **2019**, *140*, 749−760.

(21) Wu, J.; Zeng, R. J. Biomimetic Regulation of Microbially Induced Calcium Carbonate Precipitation Involving Immobilization of Sporasarcina pasteurii by Sodium Alginate. *Cryst. Growth Des.* **2017**, *17*, 1854−1862.
(22) Zhang, Y.; Bi, X.; Li, P.; Wu, Y.; Yuan, G.; Li, X.; Zuo, Y. Sodium silicate/magnesium chloride compound-modified Chinese fir wood. *Wood Sci. Technol.* **2021**, *55*, 1781−1794.
(23) Sonia, A.; Priya Dasan, K. Chemical, morphology and thermal evaluation of cellulose microfibers obtained from Hibiscus sabdariffa. *Carbohydr. Polym.* **2013**, *92*, 668−674.
(24) Tjeerdsma, B. F.; Militz, H. Chemical changes in hydrothermal treated wood: FTIR analysis of combined hydrothermal and dry heat-treated wood. *Holz. Roh. Werkst.* **2005**, *63*, 102−111.
(25) He, Q.; Huang, Z.; Liu, Y.; Chen, W.; Xu, T. Template-directed one-step synthesis of flowerlike porous carbonated hydroxyapatite spheres. *Mater. Lett.* **2007**, *61*, 141−143.
(26) Donners, J. J. J. M.; Meijer, E. W.; Nolte, R. J. M.; Roman, C.; Schenning, A. P. H. J.; Sommerdijk, N. A. J. M.; Heywood, B. R. Amorphous calcium carbonate stabilised by poly (propylene imine) dendrimers. *Chem. Commun.* **2000**, 1937−1938.
(27) Russo, R.; Malinconico, M.; Santagata, G. Effect of cross-linking with calcium ions on the physical properties of alginate films. *Biomacromolecules* **2007**, *8*, 3193−3197.
(28) Hai, T. A. P.; Sugimoto, R. Fabrication of multicolor fluorescent polyvinyl alcohol through surface modification with conjugated polymers by oxidative polymerization. *Appl. Surf. Sci.* **2018**, *443*, 1−10.
(29) Gan, W.; Chen, C.; Wang, Z.; Song, J.; Kuang, Y.; He, S.; Mi, R.; Sunderland, P.; Hu, L. Dense, Self-Formed Char Layer Enables a Fire-Retardant Wood Structural Material. *Adv. Funct. Mater.* **2019**, *29*, 1807444.
(30) Sergeeva, A.; Vikulina, A. S.; Volodkin, D. Porous Alginate Scaffolds Assembled Using Vaterite $CaCO_3$ Crystals. *Micromachines (Basel)* **2019**, *10*, 357−378.
(31) Kong, L.; Guan, H.; Wang, X. In Situ Polymerization of Furfuryl Alcohol with Ammonium Dihydrogen Phosphate in Poplar Wood for Improved Dimensional Stability and Flame Retardancy. ACS Sustain. *Chem. Eng.* **2018**, *6*, 3349−3357.
(32) Saiful Islam, M..; Hamdan, S.; Jusoh, I.; Rezaur Rahman, M..; Ahmed, A. S. The effect of alkali pretreatment on mechanical and morphological properties of tropical wood polymer composites. *Mater. Des.* **2012**, *33*, 419−424.
(33) Zhou, X.; Fu, Q.; Zhang, Z.; Fang, Y.; Wang, Y.; Wang, F.; Song, Y.; Pittman, C. U.; Wang, Q. Efficient flame-retardant hybrid coatings on wood plastic composites by layer-by-layer assembly. *Clean. Prod.* **2021**, *321*, 128949−128958.

https://doi.org/10.1021/acsomega.2c03960
ACS Omega 2022, 7, 29465−29474